Electronic Supporting Information

A porous and photoactive Ti-MOF based on a novel tetranuclear [Ti$_2$Tb$_2$] cluster

Qingxia Yao,*[a] Xuze Pan,[a] Xuezhen Si,[a] Xin Wang,[a] Xiaoying Zhang,[a] Jinle Hou,[a] Jie Su,*[b] Yi Qiu,[b] Jun Li*[a]

a. *School of Chemistry and Chemical Engineering, and Shandong Provincial Key Laboratory/Collaborative Innovation Center of Chemical Energy Storage and Novel Cell Technology, Liaocheng University, Liaocheng 252000, China. E-mail: yaoqingxia@lcu.edu.cn; Junli@lcu.edu.cn*
b. *College of Chemistry and molecular engineering, Peking University, Beijing, 100871,PR China. E-mail: jie.su@pku.edu.cn*

S1 Materials and Instruments.

All chemicals were commercially available and used without further purification. IR spectra were recorded on a Nicolet-iS50 FT-IR spectrophotometer with KBr pellets in the region of 4000-400 cm^{-1}. UV-vis absorption spectra were carried out on a Shimadzu UV-2600 spectrometer. The powder X-ray diffraction (PXRD) data were collected on a Rigaku SmartLab 9 kW Advance diffractionmeter with Cu-Kα radiation (λ=1.5418 Å) at 298 K. Thermogravimetric analysis (TGA) and mass spectrum was performed under nitrogen atmosphere on a Netzsch STA 449F5-QMS403C simultaneous TG/DSC-QMS analyzer with a heating rate of 20 °C/min. N$_2$ and CO$_2$ adsorption isotherms were measured on a Micromeritics ASAP 2460 system. The sample were degassed at 150 °C for 12 h prior to the measurements. SEM-Energy-dispersive X-Ray analysis (EDX) Particle morphologies and dimensions were studied with a Thermo Fisher Scientific FIB-SEM GX4 scanning electron microscope at an accelerating voltage of 20 kV. Valence band X-ray photoelectron spectroscopy (VB XPS) was obtained using a Thermo Scientific K-Alpha+ spectrometer equipped with a monochromatic Al Kα X-ray source. The electron spin resonance (ESR) experiments were carried out at X-band frequency (9.8 GHz) recorded with an electron spin resonance spectrometer (EPR-200Plus) at 298 K. Inductively Coupled Plasma-Mass Spectrometry (ICP-MS) experiments were performed at ThermoFisher iCAPRQ.

S2 Synthesis of LCU-505.

Synthesis of [Ti$_2$Tb$_2$(μ$_3$-O)$_2$(μ$_2$-η$_1$:η$_1$-CH$_3$COO)$_2$(H$_2$O)$_4$(TATB)$_{8/3}$]·(DMF)$_5$·(H$_2$O)$_5$ (LCU-505): A mixture of Ti(O^{i}Pr)$_4$ (21.3 mg), TbCl$_3$·(H$_2$O)$_6$ (16.4 mg), H$_3$TATB (65.8 mg), DMF (3.0 mL), acetic acid (1.6 mL) was sealed in a 23.0 mL Teflon-lined stainless-steel container, which was heated at 120 ºC for 48 hours to afford cubic crystals embedded in gel-like suspension. The crystals were collected by centrifuge, washed thoroughly by fresh DMF, and then dried in air at room temperature. Yield > 36 %. IR /cm^{-1} (KBr): 3412 (br), 2927 (w), 1663 (m), 1561 (m), 1519 (s), 1355 (w), 1174 (w), 1089 (m), 1016 (m), 835 (s), 777 (w), 700 (w), 682 (w), 597 (w), 515(w). Elemental analysis (wt%) for C$_{83}$H$_{91}$N$_{13}$O$_{36}$Tb$_2$Ti$_2$: exp. C 44.41, H 4.05, N 8.05; calcd. C 44.37, H 3.63, N 7.76.

Table S1 The reported Ti-MOFs with various Ti-O clusters

Entry	Metalcluster/core	Ligands	Materials	Surface area	Ref
1	TiO_6	H_3ondc	ZTOF-2	$S_{BET} = 1878\ m^2\ g^{-1}$	1
2	TiO_6	DOBDC	NTU-9		2
3	TiO_6	DOBDC	MIL-167		3
4	TiO_6	DOBDC	MIL-168		3
5	TiO_6	H_2Cl_2dhbq	1-Ti		4
6	TiO_6	H_4bdha	MUV-11	$S_{BET} = 756\ m^2\ g^{-1}$	5
7	$TiO_4(\mu_2\text{-}O)_2$	H_4TBAPy	ACM-1	$S_{BET} = 1212\ m^2\ g^{-1}$	6
8	$TiO_6(\mu_2\text{-}O)$	BPDC	COK-47	$S_{BET} = 573\ m^2\ g^{-1}$	7
9	$TiO_6(\mu_2\text{-}O)$	BDC	COK-47-bdc		7
10	$TiO_6(\mu_2\text{-}O)$	BPYRDC	COK-47-bpyrdc		7
11	$Ti(C_2O_2)_3$	THO	Ti-CAT-5	$S_{BET} = 450\ m^2\ g^{-1}$	8
12	Ti_2O_{11}	DOBDC	MIL-169		3
13	Ti_3O	BDC	Ti-MIL-101		9
14	$Ti_3(OH)_2$	BPDC	Ti$_3$-BPDC	$S_{BET} = 636\ m^2\ g^{-1}$	10
15	$Ti_3(\mu_3\text{-}O)$	H_2cdc	COK-69	$S_{BET} = 29.13\ m^2\ g^{-1}$	11
16	$Ti_3(\mu_3\text{-}O)$	BTC	MIL-100(Ti)	$S_{BET} = 1321\ m^2\ g^{-1}$	12
17	$Co_2Ti(\mu_3\text{-}O)$	H_3obdc	CTOF-1	$S_{BET} = 637\ m^2\ g^{-1}$	13
18	$Co_2Ti(\mu_3\text{-}O)$	BDC	CTOF-2	$S_{BET} = 618\ m^2\ g^{-1}$	13
19	$Co_2Ti(\mu_3\text{-}O)\ (COO)_6$	ABTC	PFC-20-Co$_2$Ti		14
20	$Ni_2Ti(\mu_3\text{-}O)\ (COO)_6$	ABTC	PFC-20-Ni$_2$Ti		14
21	$Mn_2Ti(\mu_3\text{-}O)\ (COO)_6$	ABTC	PFC-20-Mn$_2$Ti		14
22	$Co_2Ti(\mu_3\text{-}O)$	BDC TPT	Co$_2$Ti-bdc-tpt	$S_{BET} = 1369.8\ m^2\ g^{-1}$	15
23	$Mg_2Ti(\mu_3\text{-}O)$	BDC PTP	Mg$_2$Ti-bdc-tpt	$S_{BET} = 1460.6\ m^2\ g^{-1}$	15
24	$Mg_2Ti(\mu_3\text{-}O)$	BDC TPPy	Mg$_2$Ti-bdc-tppy	$S_{BET} = 1599.1\ m^2\ g^{-1}$	15
25	$Mg_2Ti(\mu_3\text{-}O)$	BDC TPBz	Mg$_2$Ti-bdc-tpbz	$S_{BET} = 1661.7\ m^2\ g^{-1}$	15
26	$Zn_3Ti(\mu_3\text{-}OH)$	H_3obdc	ZTOF-1	$S_{BET} = 1045\ m^2\ g^{-1}$	16
27	$Ti_2Ca_2(\mu_3\text{-}O)_2(H_2O)_4$	BTC	MUV-10	$S_{BET} = 1041\ m^2\ g^{-1}$	17
28	$Ti_2Ca_2(\mu_3\text{-}O)_2(H_2O)_4$	H_3BTB	LCU-402	$S_{BET} = 1460\ m^2\ g^{-1}$	18
29	$Ti_2Tb_2(\mu_3\text{-}O)_2(H_2O)_4$	H_3TATB	LCU-505	$S_{BET} = 882.4\ m^2\ g^{-1}$	This work
30	Zr_6Ti_4	H4TBAPy	NU-1012		19
31	$[Ti_5(OAc)_2(OH)_6]_n$	5,10,15,20-Tetra(p-benzoato) porphyrin (TBP or TCPP)	Ti-TBP	$S_{BET} = 527.7\ m^2\ g^{-1}$	20
32	$(Ti_6O_9)_n$	mdip	MIL-177-HT	$S_{BET} = 690\ m^2\ g^{-1}$	21
33	$Ti_6(\mu_3\text{-}O)_6(\mu_3\text{-}OH)_6$	H_3TCA	ZSTU-1	$S_{BET} = 536\ m^2\ g^{-1}$	22
34	$Ti_6(\mu_3\text{-}O)_6(\mu_3\text{-}OH)_6$	H_3BTB	ZSTU-2	$S_{BET} = 628\ m^2\ g^{-1}$	22
35	$Ti_6(\mu_3\text{-}O)_6(\mu_3\text{-}OH)_6$	H_3BTCA	ZSTU-3	$S_{BET} = 861\ m^2\ g^{-1}$	22
36	Ti_6O_6	4-Aminobenzoate (AB) BDA	MOF-901	$S_{BET} = 550\ m^2\ g^{-1}$	23
37	Ti_6O_6	AB and BPDA	MOF-902	$S_{BET} = 400\ m^2 g^{-1}$	24
38	Ti_7O_6	TCPP	PCN-22	$S_{BET} = 1284\ m^2\ g^{-1}$	25
39	Ti_8O_8	BPDC	UCFMOF-2	$S_{BET} = 354 m^2\ g^{-1}$	26
40	Ti_8O_8	TPDC	UCFMOF-3	$S_{BET} = 1777 m^2\ g^{-1}$	26

41	Ti_8O_8	QPDC	UCFMOF-4	S_{BET} =2430 m^2 g^{-1}	26
42	Ti_8O_8	TPDC DATP	UCFMTV-3-x%		26
43	Ti_8O_8	QPDC DAQP	UCFMTV-4-x%		26
44	$Ti_8O_8(OH)_4$	H_2BDC	MIL-125	S_{BET} = 1550 m^2 g^{-1}	27
45	$Ti_8O_8(OH)_4$	NH_2-BDC	NH_2-MIL-125	S_{BET} = 1302 m^2 g^{-1}	28
46	$Ti_8(\mu_2\text{-}O)_8(OAC)_8$	BTC	MIP-207	S_{BET} = 570 m^2 g^{-1}	29
47	$Ti_8Zr_2O_{12}$	BDC	PCN-415	S_{BET} = 1550 m^2 g^{-1}	30
48	$Ti_8Zr_2O_{12}$	NDC	PCN-416	S_{BET} = 1337 m^2 g^{-1}	30
49	$Ti_{12}O_{15}$	mdip	MIL-177-LT	S_{BET} = 730 m^2 g^{-1}	21
50	$Ti_n(\mu_2\text{-}O)_n$	TCPP	DGIST-1	S_{BET} = 1957.3 m^2 g^{-1}	31
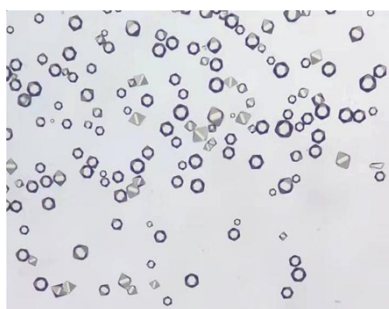
Fig. S1 Photographs of single crystals of LCU-505.

S3 Scanning Electron Microscopy (SEM-EDX).

Particle morphologies, dimensions, and SEM-Energy-dispersive X-Ray analysis (EDX) of LCU-505 solids were studied with a Thermo Fisher Scientific FIB-SEM GX4 scanning electron microscope at an accelerating voltage of 20 kV. Mapping of LCU-505 showing Ti (roseo) and Tb (green) confirms that element distribution is homogeneous.
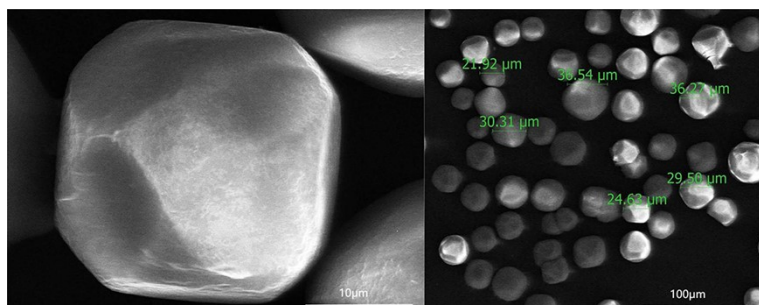
Fig. S2 Scanning Electron Microscopy (SEM) images of LCU-505.
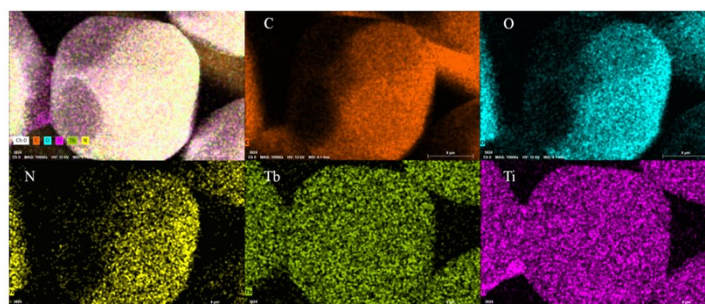
Fig. S3 Mapping of LCU-505 showing Ti (pink) and Tb (yellow).

S4 Single-crystal X-ray diffraction analysis of LCU-505.

SCXRD data for LCU-505 was carried out on a Mercury single crystal diffractometer equipped with graphite-monochromatic Ga Ka radiation (λ=1.3405 Å) at 100 K. All absorption correction was applied using multi-scan technique. The crystal structure of LCU-505 was solved by the direct method and refined through full-matrix least-squares techniques method on F^2 using the SHELXTL 2018 and Olex2 crystallographic software package. Guest molecules could not be located in the void due to very weak diffraction. Disordered solvents, including 30 DMF molecules and 30 water molecules, were removed from one unit cell by the SQUEEZE process.[32] Full crystallographic data for LCU-505 has been deposited with the CCDC 2264522.

Inspection of the data in the hkl file shows that reflections with (h+k+l = 2n) are all strong as would be expected for an I-lattice; the reflections with (h+k+l = 2n+1) are for the most part much weaker but many appear to be well determined and thus cannot be ignored. Therefore, the choice of space group Pm-3n may indeed be the better one, rather than Im-3m.

When solving the structure, we found ambiguous electron density cloud around the planar [Ti$_2$Tb$_2$] cluster, and two strong electron-density peaks adjacent to the assigned Ti and Tb atom, indicating severe disorder of the [Ti$_2$Tb$_2$] cluster. The [Ti$_2$Tb$_2$] cluster was split into two parts (part A and B) and refined without restraint on the occupancy, finally giving the refined occupancy value of 0.732 for part A. The two disordered parts are perpendicular to each other and approximately imposed by crystallographic mirror planes (101) and (10-1).

Not unexpectedly in this disordered heavy-atom structure that there were problems with H-atom locations. H atoms bonded to carbon atoms were placed geometrically and no allowance was possible for H atoms bonded to oxygen atoms. Note that even although we could not locate the H atoms of coordinated water molecules, the contributions of these missing atoms are included in the formula in Table S2.

Table S2 Crystal data and structure refinements for LCU-505

	LCU-505
Empirical formula	$C_{41.5}H_{45.5}N_{6.5}O_{18}TbTi$
Formula weight	1130.13
Crystal system	cubic
Space group	*Pm-3n*
a/Å	25.9298(2)
b/Å	25.9298(2)
c/Å	25.9298(2)
α/°	90
β/°	90
γ/°	90

Volume/Å^3	17434.0(4)
Z	12
ρ_{calc}g/cm^3	1.292
μ/mm^{-1}	1.388
$F(000)$	5304.0
2θ range for data collection/°	3.142 to 50.03
Index ranges	$-13 \leq h \leq 27$, $-28 \leq k \leq 15$, $-30 \leq l \leq 15$
GoF on F^2	1.250
Final R indexes [I> =2σ (I)]	R$_1$ = 0.1114, wR$_2$ = 0.3084
Final R indexes [all data]	R$_1$ = 0.1375, wR$_2$ = 0.3339
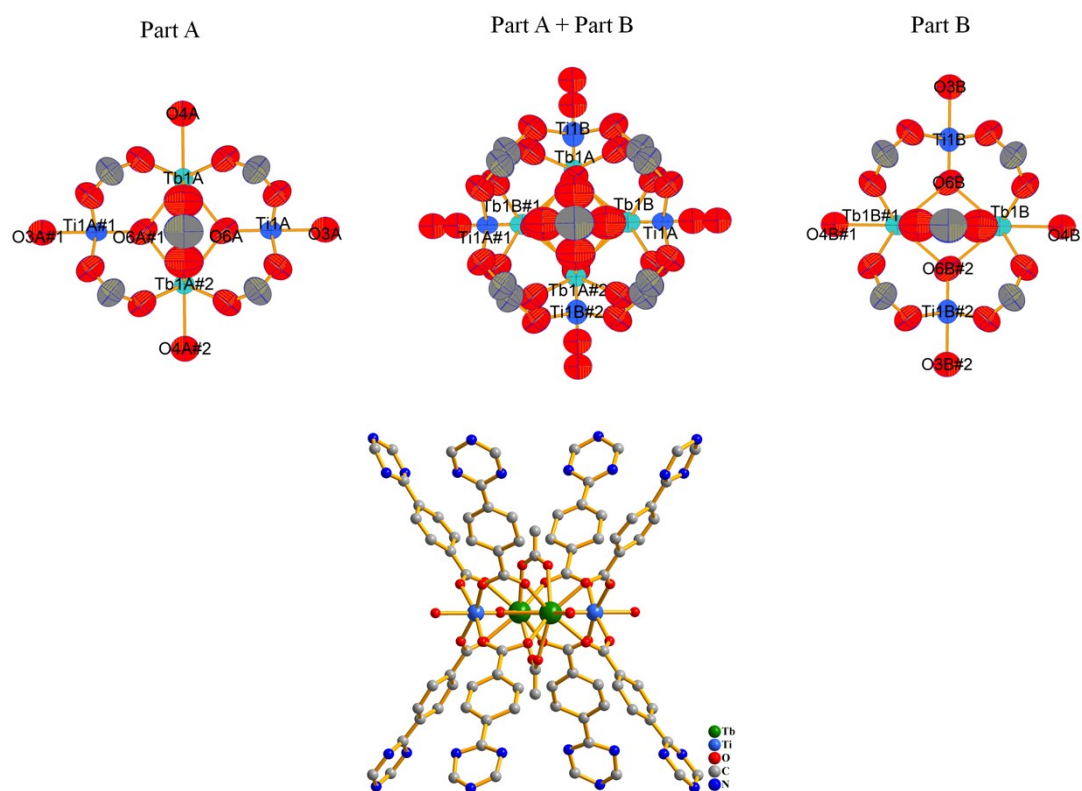
Fig. S4 The disorder of the Ti$_2$Tb$_2$ cluster and the coordination environment around 8-c cluster.
Symm. Code: #1 = -x+1, -y, z; #2 = x, -y, 1-z.
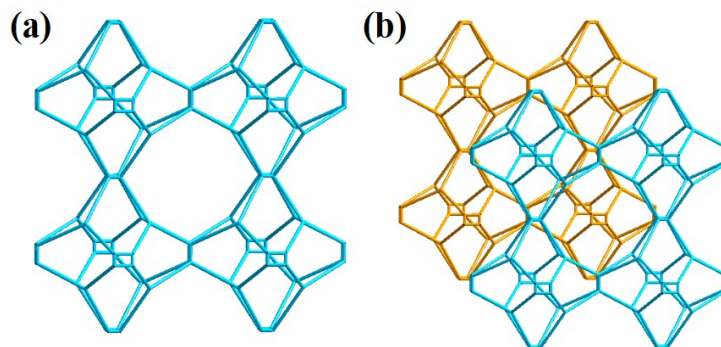
Fig. S5 (a) Topological structure of the (3,8)-connected cubic network. (b) Topological structure of the interpenetrated networks.
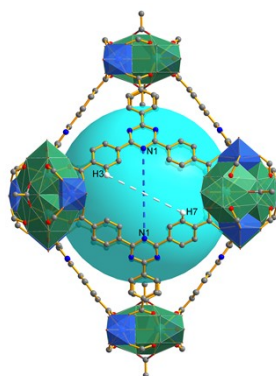
Fig. S6 Distances of N1···N1 (symm. code: x, y, 1-z) (5.7 Å) and H3 (symm. code: x, y+1, z-1)···H7 (symm. code: x, y, 1-z) (5.6 Å) on the cage.

S5 Inductively Coupled Plasma-Mass Spectrometry (ICP-MS) analysis.

Table S3 ICP analysis results of LCU-505

LCU-505	Tb wt %	Ti wt%	Tb:Ti (mol/mol)
1	14.72 %	4.51 %	0.98:1
2	14.65 %	4.47 %	0.99:1
3	14.56 %	4.32 %	1.02:1
average	14.64 %	4.43 %	1:1

S6 The PXRD patterns of LCU-505.
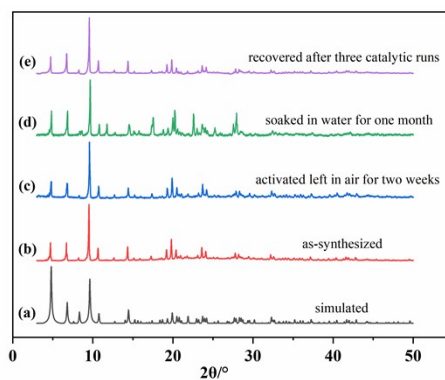
Fig. S7 The PXRD patterns of LCU-505 (a) simulated. (b) as-synthesized. (c) activated left in air for two weeks. (d) soaked in water for one month. (e) recovered after three catalytic runs.

S7 Thermogravimetric analysis.

Thermogravimetric analysis (TGA) was performed under nitrogen atmosphere on a Netzsch STA 449F5-QMS403C. TGA plot (black line) shows the LCU-505 loses all solvents (water, DMF) with a weight loss of 22.1 % before 310 °C. Then, with clear plateau, it started to decompose.
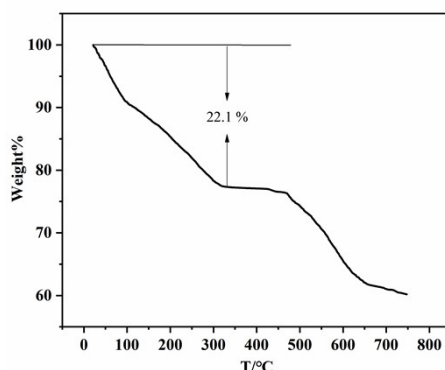
Fig. S8 TGA plot of as-synthsized LCU-505.

S8 LCU-505 Pore size distribution.

N_2 and CO_2 adsorption isotherms were measured on a Micromeritics ASAP 2460 system. The sample were degassed at 150 °C for 12 h prior to the measurements. The specific surface area was calculated from the data in the adsorption branch at p/p_0 = 0.05-0.30. The total pore volume was calculated from the uptake at p/p_0 of 0.995. CO_2 adsorption isotherms was recorded at 273 and 298 K. Pore size distribution was analysed by using the solid density functional theory (NLDFT) for the adsorption branch assuming a cylindrical pore model.
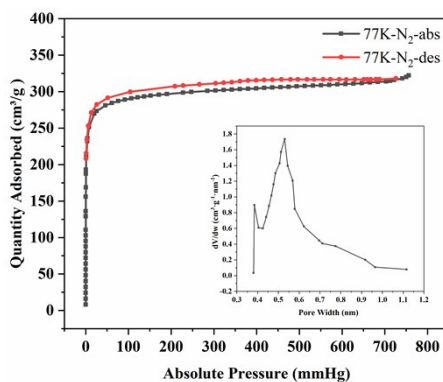
Fig. S9 LCU-505 adsorption curve and pore size distribution.

S9 Isosteric heat of CO_2 adsorption (Qst).

The adsorption heat (Qst) of hydrogen for the desolvated LCU-505 is fitted by Virial method using the data obtained from 273 K and 298 K with the following Equation:

$$Ln(P) = Ln(N) + \frac{1}{T}\sum_{i=0}^{m} a_i * N_i + \frac{1}{T}\sum_{j=0}^{n} a_j * N_j$$

N: adsorbed quantity (mg/g);

P: pressure (mmHg);

T: temperature (K);

ai, bj: constant;

R: 8.314 J·mol^{-1}·K^{-1};

The isosteric enthalpy of adsorption (Qst):

$$Q_{st} = Ln(P) = -R * \sum_{i=0}^{m} a_i * N_i$$

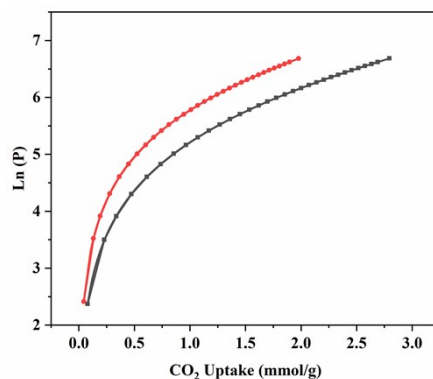**Fig. S10** Nonlinear curve fitting of CO_2 sorption isotherms for LCU-505 at 273 K and 298 K.

Table S4 Fit curve equation and factor.

		Value	Standard Error
	a0*	-2052.06378	3.612
	a1*	282.08312	7.66815
	a2*	-70.47062	5.05948
	a3*	4.36563	3.89753
273K	a4*	-0.54681	1.53172
	a5*	0.03094	0.21701
	b0*	12.39692	0.01251
	b1*	-0.64776	0.02635
	b2*	0.18791	0.01202
	k	273	0
	a0*	-2052.06378	3.61267
	a1*	282.08312	7.66815
	a2*	-70.47062	5.05948
	a3*	4.36563	3.89753
	a4*	-0.54681	1.53172
298K	a5*	0.03094	0.21701
	b0*	12.39692	0.01251
	b1*	-0.64776	0.02635
	b2*	0.18791	0.01202
	k	298	0

$$y = Ln(x) + 1/k * (a0 + a1*x + a2*x^2 + a3*x^3 + a4*x^4 + a5*x^5) + (b0 + b1*x + b2*x^2)$$

Isosteric heat of CO_2 adsorption (Qst) was calculated by using the viral equation based on the isotherms at 273 K and 298 K.
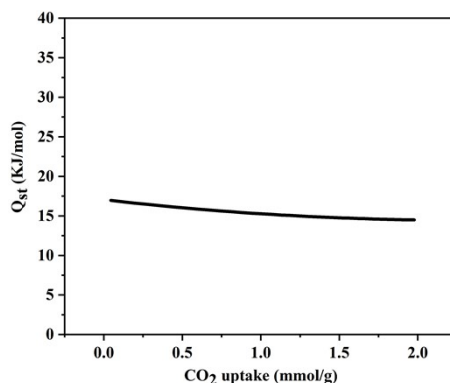
Fig. S11 Isosteric heat of adsorption (Q_{st}) calculated by the viral method.

S10 Time-dependent photocurrent curve under the visible light radiation.

Photocurrent-time plots of LCU-505 were recorded on a CHI660E electrochemistry workstation equipped with a three-elcetrode setup. A Pt wire, a Ag/AgCl electrode, and a sample-coated ITO were used as the auxiliary, reference, and working electrodes respectively. For the preparation of the working electrode, 4.0 mg of powdered LCU-505 was dispersed in a mixed ethanol/Nafion solution, followed by an ultrasonic treatment. Next, this slurry was dropped onto a pre-polished ITO substrate and died at room temperature. The electrolyte was 0.1 M KCl aqueous solution. A 300 W Xe lamp with a 420 nm filter was used as the simulated visible light.

S11 The VB-XPS of LCU-505.
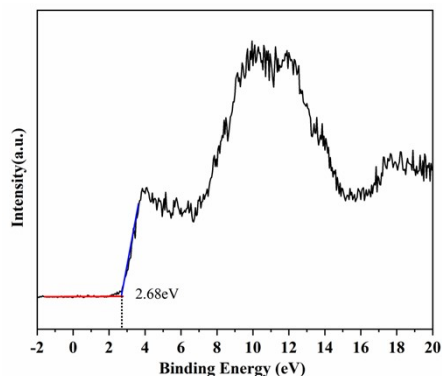
Fig. S12 The VB-XPS of LCU-505.

S12 Band structure and DOS of LCU-505.

The electronic structures of the LCU-505 were calculated by density functional theory (DFT) encoded in the Vienna ab initio simulation package (VASP). Perdew-Burke-Ernzerhof (PBE) functional in the generalized gradient approximation (GGA) was adopted to describe the exchange-correlation energy. The kinetic energy cutoff of 500 eV and the Monkhorst-Pack k-point sampling of $2 \times 2 \times 2$ were elected to perform numerical integration in the Brillouin zone. We use LSDA+ U method for the 4f states due to the strong correlation of rare earth elements.
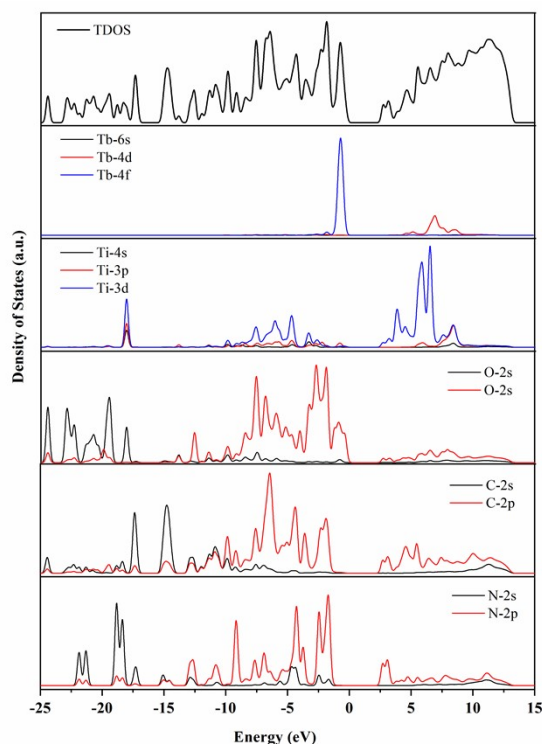
Fig. S13 DFT calculated band structures for LCU-505 and their derivatives.

S13 The photocatalytic oxidation performances of LCU-505 towards organic dyes.

The photocatalyst sample (20 mg) and different types of dye aqueous solution (10 mg·L⁻¹, 50 mL) were placed in a photoreactor. To reach the adsorption-desorption equilibrium, the mixutre was stirred for half an hour in the dark. Then, the solution was exposed to a 400 W metal halide lamp placed at a distance of 12 cm in air. An equal amount (2.5 mL) of the solution was removed from the photoreactor at predetermined intervals and centrifuged. The residual dye concentration in the supernatant was determined by UV-vis spectrophotometer. During recycle experiments, the catalyst was easily retrieved by centrifuge and reused in next run.

Table S5 The of dye molecule size of methylene blue (MB) and methylene blue (MLB)

Dye	Structure	Charge	Dimensions(Å)	3D molecular structure
methyl blue (MB)		-2	25.38×15.88×9.62	
methylene blue (MLB)		+1	15.68×7.87×4.02	

The calculated dye molecule size is larger than the pore size of LCU-505. Therefore, the

degradation of dye molecules such as methyl blue and methylene blue should take place on the surface of Ti-MOF.

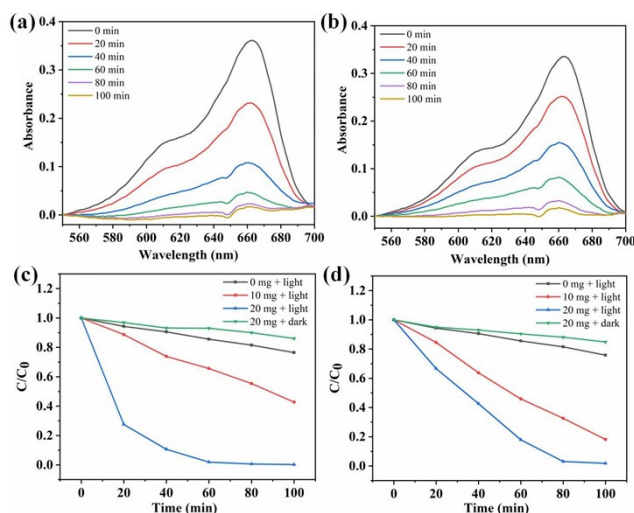**S14 The UV-vis absorption spectra of the photocatalytic process.**

Figure S14. The UV-vis absorption spectra of MB (a), MLB (b) recorded at various times during the photocatalytic process, the photocatalytic oxidation performances of LCU-505 towards MB (c), MLB (d) under different catalyst loading and light illumination.

Table S6 The MOFs related to the catalytic degradation of methylene blue (MLB).

| MOF	Dye	Studied conditions	Catalytic (%)	Ref
MIL-53	MLB	20 min, UV–vis light, H_2O_2	99 %	33
HPU-3	MLB	60 min, H_2O_2	97.2 %	34
Mn(dmtdc)	MLB	70 min, UV light	90.8 %	35
[Cu (OH) Cl (itp) (bdc)](NO) (OH)	MLB	90 min, H_2O_2 , 300 W Xe	92.5 %	36
ZIF-8	MLB	120 min, 500 W Hg	83.2 %	37
Cd-TCAA	MLB	171 min, 500 W Xe	81 %	38
Zr-MOFs-PUF	MLB	50 h, pH = 9, 25 °C	97.57 %	39
LCU-505	MLB	100 min, 300 W Xe	complete	This work
MOF-74(Zn)-Ti MOF-74(Mg)-Ti	MLB	3min, 300 W Xe	98 %	40
[Me$_2$NH$_2$][Sr$_2$(TCPP) (OAc)(H$_2$O)]·2DMA	MLB	22 min, DMA, O_2 300 W Xe	99 %	41
NTU-9(Ti)	MLB/ RB	20/80 min	complete	2

Notes: MLB = methylene blue
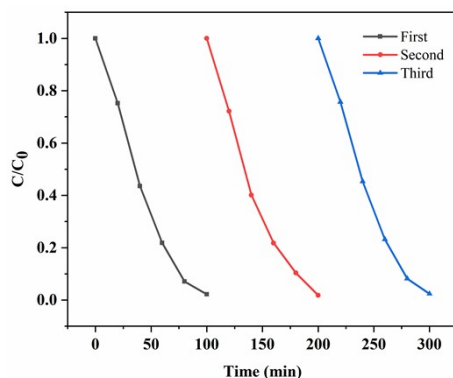
Figure S15. The reusability on LCU-505 for photo-degradation of MB under under the alternate visible light radiation ($\lambda > 420$ nm).

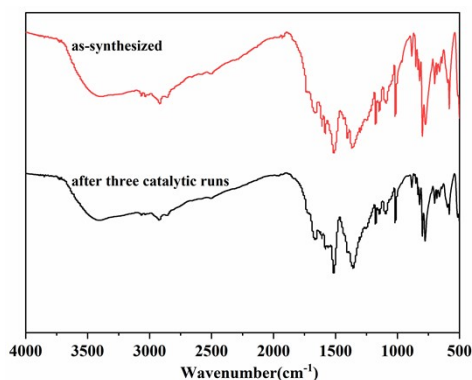## S15 Fourier-Transform infrared spectrum.

Figure S16 The FT-IR spectrum of LCU-505 as-synthesized and after three catalytic runs.

S16 EPR spectra of the solid LCU-505.

The ESR measurements of LCU-505 solids before and after irradiation were carried out at X-band frequency (9.8 GHz) at 298 K.
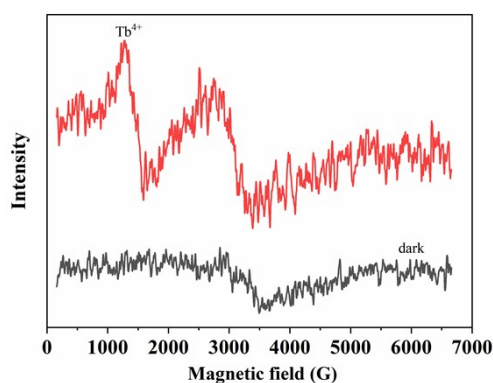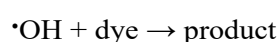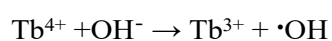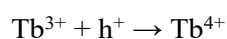

Figure S17. EPR spectra of the LCU-505 before and after irradiation (Xe 300W, 5 min) at 298 K.

EPR of the non-Kramers ion Tb^{3+} ($4f^8$, $^7F_6$) has been observed only below 30 K.[42-44] In contrast, EPR of Tb^{4+} ($4f^7$, $^8S_{7/2}$) consists of hyperfine signals at liquid helium temperature and can be observed even at room temperature.[44,45]
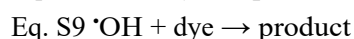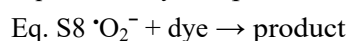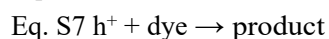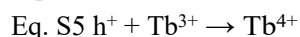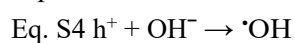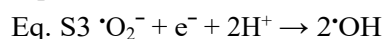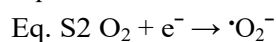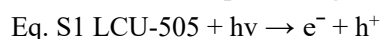
Here, in order to detect both valence states of terbium (Tb^{3+} and Tb^{4+}), the ESR

measurements of LCU-505 solids before and after irradiation were carried out at X-band frequency (9.8 GHz) at 298 K (S 16). ESR spectra at 298 K are shown in Fig. S17. LCU-505 before irradiation (in the dark) is ESR silent, as explained above. In contrast, LCU-505 after visible-light irradiation is ESR active and two new ESR signals appears in the spectrum. The ESR signal at g = 2.0 can be ascribed to hole (h^+) centers caused by electron-hole separation under irradiation.[46] The ESR signal at g = 5.0 is assigned to Tb^{4+} ions. This result is also consistent with ESR feature of Tb^{4+} in glasses at room temperature.[44]

The ESR results indicates the generation of photo-induced Tb^{4+} ions. It has been reported by Li and coworkers that the formation of Tb^{4+}/Tb^{3+} can enhance photo-activity of a $Tb_2O_3/g\text{-}C_3N_4$ composite photocatalyst.[47] Similarly, the in-built redox centers of Tb^{4+}/Tb^{3+} in LCU-505 might facilitate the separation of charge carriers and offer a new path to produce more hydroxyl radicals ($^\bullet OH$) to improve the photocatalytic property. The Tb^{4+}/Tb^{3+} involved photo-degradation reaction can be described as follows:

$Tb^{3+} + h^+ \rightarrow Tb^{4+}$

$Tb^{4+} + OH^- \rightarrow Tb^{3+} + {}^\bullet OH$

$^\bullet OH + dye \rightarrow product$

S17 The involved photo-degradation reactions.

Eq. S1 LCU-505 + hv $\rightarrow e^- + h^+$

Eq. S2 $O_2 + e^- \rightarrow {}^\bullet O_2{}^-$

Eq. S3 $^\bullet O_2{}^- + e^- + 2H^+ \rightarrow 2{}^\bullet OH$

Eq. S4 $h^+ + OH^- \rightarrow {}^\bullet OH$

Eq. S5 $h^+ + Tb^{3+} \rightarrow Tb^{4+}$

Eq. S6 $Tb^{4+} + OH^- \rightarrow {}^\bullet OH + Tb^{3+}$

Eq. S7 $h^+ + dye \rightarrow product$

Eq. S8 $^\bullet O_2{}^- + dye \rightarrow product$

Eq. S9 $^\bullet OH + dye \rightarrow product$

References

1. K. Hong, H. Chun, *Chem. Commun.*, 2013, **49**, 10953.

2. J. Gao, J. Miao, P.-Z. Li, W. Y. Teng, L. Yang, Y. Zhao, B. Liu, Q. Zhang, *Chem. Commun.*, 2014, **50**, 3786-3788.

3. H. Assi, L. C. P. Pérez, G. Mouchaham, F. Ragon, M. Nasalevich, N. Guillou, C. Martineau, H. Chevreau, F. Kapteijn, J. Gascon, P. Fertey, E. Elkaim, C. Serre, T. Devic, *Inorg. Chem.*, 2016, **55**, 7192.

4. M. E. Ziebel, L. E. Darago, J. R. Long, *J. Am. Chem. Soc.*, 2018, **140**, 3040.

5. N. M. Padial, J. Castells-Gil, N. Almora-Barrios, M. Romero-Angel, I. d. Silva, M. Barawi, A. García-Sánchez, V. A. d. l. P. O'Shea, C. Martí-Gastaldo, *J. Am. Chem. Soc.*, 2019, **141**, 13124-13133.

6. A. Cadiau, N. Kolobov, S. Srinivasan, M. G. Goesten, H. Haspel, A. V. Bavykina, M. R. Tchalala, P. Maity, A. Goryachev, A. S. Poryvaev, M. Eddaoudi, M. V. Fedin, O. F. Mohammed,

J. Gascon, *Angew. Chem. Int. Ed.*, 2020, **59**, 13468-13472.

7. S. Smolders, T. Willhammar, A. Krajnc, K. Sentosun, M. T. Wharmby, K. A. Lomachenko, S. Bals, G. Mali, M. B. J. Roeffaers, D. E. D. Vos, B. Bueken, *Angew. Chem. Int. Ed.*, 2019, **58**, 9160-9165.

8. N. T. T. Nguyen, H. Furukawa, F. Gandara, C. A. Trickett, H. M. Jeong, K. E. Cordova, O. M. Yaghi, *J. Am. Chem. Soc.*, 2015, **137**, 15394-15397.

9. J. A. Mason, L. E. Darago, W. W. Lukens, Jr, J. R. Long, *Inorg. Chem.*, 2015, **54**, 10096-10104.

10. X. Feng, Y. Song, J. S. Chen, Z. Li, E. Y. Chen, M. Kaufmann, C. Wang, W. Lin, *Chem. Sci.*, 2019, **10**, 2193-2198.

11. B. Bueken, F. Vermoortele, D. E. P. Vanpoucke, H. Reinsch, C.-C. Tsou, P. Valvekens, T. D. Baerdemaeker, R. Ameloot, C. E. A. Kirschhock, V. V. Speybroeck, J. M. Mayer, D. D. Vos, *Angew. Chem. Int. Ed.*, 2015, **127**, 14118 -14123.

12. J. Castells-Gil, N. M. Padial, N. Almora-Barrios, I. d. Silva, D. Mateo, J. Albero, H. García, C. Martí-Gastaldo, *Chem. Sci.*, 2019, **10**, 4313-4321.

13. K. Hong, W. Bak, D. Moon, H. Chun, *Cryst. Growth Des.*, 2013, **13**, 4066-4070.

14. L. Li, Z.-B. Fang, W. Deng, J.-D. Yi, R. Wang, T.-F. Liu, *CCS Chem.*, 2021, **3**, 2839-2849.

15. H. Yang, Y. Wang, R. Krishna, X. Jia, Y. Wang, A. N. Hong, C. Dang, H. E. Castillo, X. Bu, P. Feng, *J. Am. Chem. Soc.*, 2020, **142**, 2222-2227.

16. K. Hong, W. Bak, H. Chun, *Inorg. Chem.*, 2013, **52**, 5645-5647.

17. J. Castells-Gil, N. M. Padial, N. Almora-Barrios, J. Albero, A. R. RuizSalvador, J. Gonzlez-Platas, H. García, C. Martí-Gastaldo, *Angew. Chem. Int. Ed.*, 2018, **57**, 8453-8457.

18. X. Pan, X. Si, X. Zhang, Q. Yao, Y. Li, W. Duan, Y. Qiu, Jie Su, X. Huang, *Dalton Trans.*, 2023, **52**, 3896-3906.

19. X. Wang, K. Ma, T. Goh, M. R. Mian, H. Xie, H. Mao, J. Duan, K. O. Kirlikovali, A. E. B. S. Stone, D. Ray, M. R. Wasielewski, L. Gagliardi, O. K. Farha., *J. Am. Chem. Soc.*, 2022, **144**, 12192 -12201.

20. G. Lan, K. Ni, S. S. Veroneau, X. Feng, G. T. Nash, T. Luo, Z. Xu, W. Lin, *J. Am. Chem. Soc.*, 2019, **141**, 4204-4208.

21. S. Wang, T. Kitao, N. Guillou, M. Wahiduzzaman, C. Martineau-Corcos, F. Nouar, A. Tissot, L. Binet, N. Ramsahye, S. Devautour-Vinot, S. Kitagawa, S. Seki, Y. Tsutsui, V. Briois, N. Steunou, G.Maurin, T. Uemura, C. Serre, *Nat. Commun.*, 2018, **9**, 1660.

22. C. Li, H. Xu, J. Gao, W. Du, L. Shangguan, X. Zhang, R. Lin, H. Wu, W. Zhou, Xin. Liu, J. Yao, B. Chen, *J. Mater. Chem. A.*, 2019, **7**, 11928-11933.

23. H. L. Nguyen, F. Gándara, H. Furukawa, T. L. H. Doan, K. E. Cordova, O. M. Yaghi, *J. Am. Chem. Soc.*, 2016, **138**, 4330-4333.

24. H. L. Nguyen, T. T. Vu, D. Le, T. L. H. Doan, V. Q. Nguyen, N. T. S. Phan, *ACS Catal.,* 2017, **7**, 338-342.

25. S. Yuan, T.-F. Liu, D. Feng, J. Tian, K. Wang, J. Qin, Q. Zhang, Y.-P. Chen, M. Bosch, L. Zou, S. J. Teat, S. J. Dalgarno, H.-C. Zhou, *Chem. Sci.,* 2015, **6**, 3926-3930.

26. J. T. Bryant, M. W. Logan, Z. Chen, M. Djokic, D. R. Cairnie, D. A. Vazquez-Molina, A. Nijamudheen, K. R. Langlois, M. J. Markley, G. Pombar, A. A. Holland, J. D. Caranto, J. K. Harper, A. J. Morris, J. L. Mendoza-Cortes, T. Jurca, K. W. Chapman, F. J. Uribe-Romo, *J. Am. Chem. Soc.,* 2023, **145**, 8, 4589-4600.

27. M. Dan-Hardi, C. Serre, T. Frot, L. Rozes, G. Maurin, C. Sanchez, G. Férey, *J. Am. Chem.*

Soc., 2009, **131**, 10857-10859.

28. Y. Fu, D. Sun, Y. Chen, R. Huang, Z. Ding, X. Fu, Z. Li, *Angew. Chem. Int. Ed.*, 2012, **51**, 3364-3367.

29. S.Wang, H. Reinsch, N. Heymans, M. Wahiduzzaman, C. Martineau-Corcos, G. De Weireld, G. Maurin, C. Serre, *Matter,* 2020, **2**, 440.

30. Yuan, J. S. Qin, H. Q. Xu, J. Su, D. Rossi, Y. Chen, L. Zhang, C. Lollar, Q. Wang, H. L. Jiang, D. H. Son, H. Xu, Z. Huang, X. Zou, H. C. Zhou, *ACS Cent. Sci.*, 2018, **4**, 105.

31. Y. Keum, S. Park, Y.-P. Chen, J. Park, *Angew. Chem. Int. Ed.*, 2018, **57**, 14852-14856.

32. A. L. Spek, *Acta Cryst.*, 2015, **C71**, 9-18.

33. J.-J. Du, Y.-P. Yuan, J.-X. Sun, F.-M. Peng, X. Jiang, L.-G. Qiu, A.-J. Xie, Y.-H. Shen, J.-F. Zhu, *J. Hazard. Mater.,* 2011, **190**, 945-951.

34. Z. Xu, Q. Li, X. He, H. Li, Y. Wang, J. Cao, *Polyhedron*, 2018, **151**, 478-482.

35. X.-D. Fang, L.-B. Yang, A.-N. Dou, Y.-E. Liu, J. Yao, Q.-Q. Xu, A.-X. Zhu., *Inorganic Chemistry Communications*., 2018, **96**, 124−127.

36. T.-R. Zheng, L.-L. Qian, Min Li, Z.-X. Wang, K. Li, Y.-Q. Zhang, B.-L. Li, B. Wu, *Dalt. Trans.*, 2018, **47**, 9103-9113.

37. H.-P. Jing, C.-C. Wang, Y.-W. Zhang, P. Wang, R. Li, *RSC Adv.*, 2014, **4**, 54454-54462.

38. L. Xia, J. Ni, P. Wu, J. Ma, L. Bao, Y. Shi, J. Wang, *Dalt. Trans.*, 2018, **47**, 16551-16557.

39. J. Li, J.-L. Gong, G.-M. Zeng, P. Zhang, B. Song, W.-C. Cao ,H.-Y. Liu, S.-Y. Huan, *J. Colloid Interface Sci.*, 2018, **527**, 267-279.

40. L. Zou, D. Feng, T.-F. Liu, Y.-P. Chen, S. Yuan, K. Wang, X. Wang, S. Fordham, H.-C. Zhou, *Chem. Sci.*, 2016, **7**, 1063-1069.

41. X.-H. Chen, Y.-S. Zhang, W.-B. Li, X.-W. Guan, J.-W. Ye, L. Chen, H.-P. Wang, J. Bai, Z.-W. Mo, X.-Ming Chen, *Inorg. Chem. Front.*, 2022, **9**, 2328-2335.

42. P. A. Forrester, C. F. Hempstead, *Phys. Rev.*, 1962, **126**, 923-930.

43. M. R. Gafurov, V.A. Ivanshin, I.N. Kurkin, M.P. Rodionova, H. Keller, M. Gutmann, U. Staub, *J. Magn. Reson.*, 2003, **161**, 210-214.

44. H. Ebendorff-Heidepriem, D Ehrt, *J. Phys.: Condens. Matter*, 1999, **11**, 7627-7634.

45. R. Yu. Abdulsabirov, I. N. Kurkin, *Sov. Phys. J. Izvestia Vuz. Fizika*, 1978, **21**, 1096-1098.

46. Y. Nosaka, M. Nishikawa, A. Y. Nosaka, *Molecules*, 2014, **19**, 18248-18267.

47. X. Li, W. Li, X. Liu, H. Li, C. Ren, H. Fan, X. Ma, M. Dong, *J. Taiwan. Inst. Chem. E.*, 2021, **127**, 265-275.